ACS Energy LETTERS

Cite This: ACS Energy Lett. 2019, 4, 1073−1079

http://pubs.acs.org/journal/aelccp

LETTER

Cathode-Supported All-Solid-State Lithium−Sulfur Batteries with High Cell-Level Energy Density

Ruochen Xu,[†,‡] Jie Yue,[†] Sufu Liu,[†,‡] Jiangping Tu,[‡] Fudong Han,[*,†] Ping Liu,[*,§] and Chunsheng Wang[*,†]

[†]Department of Chemical and Biomolecular Engineering, University of Maryland, College Park, Maryland 20742, United States

[‡]State Key Laboratory of Silicon Materials, Key Laboratory of Advanced Materials and Applications for Batteries of Zhejiang Province, and School of Materials Science & Engineering, Zhejiang University, Hangzhou 310027, China

[§]Department of Nanoengineering, University of California, San Diego, La Jolla, California 92093, United States

Supporting Information

ABSTRACT: Bulk-type all-solid-state lithium batteries (ASSLBs) are being considered as a promising technology to improve the safety and energy density of today's batteries. However, current bulk-type ASSLBs suffer from low cell-level energy density due to the challenges in reducing the electrolyte thickness. In this work, we report cathode-supported ASSLBs with a thin solid electrolyte layer. Starting from a stainless steel mesh-supported Li_2S cathode, we are able to build an ASSLB with a ∼100 μm thick Li_3PS_4 electrolyte reinforced by a Kevlar nonwoven scaffold and with Li metal as the anode. The ASSLB delivers a high capacity with high rate and cycling performances at room temperature. Moreover, the unique cell design also enabled utilization of a thick cathode with a Li_2S loading of 7.64 mg cm^{-2}, providing a high cell-level energy density (excluding the current collectors) of 370.6 Wh kg^{-1} for the first cycle.

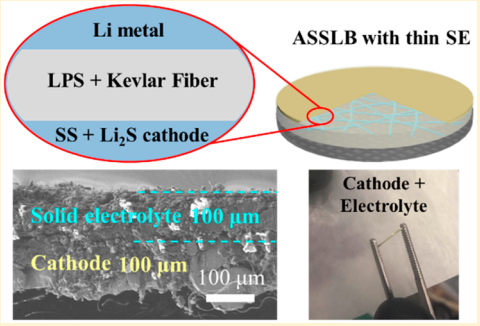

All-solid-state lithium batteries (ASSLBs) hold great potential to significantly improve the safety and energy density of today's lithium ion batteries by using nonflammable, inorganic solid electrolytes.[1−3] Solid electrolytes play a critical role in enabling ASSLBs. Among various lithium ion-conducting materials, sulfide-based solid electrolytes are one of the most promising electrolytes because of their excellent ionic conductivity and mechanical property.[4,5] The ionic conductivities of several sulfide electrolytes are comparable with or even higher than that of the organic liquid electrolyte,[4−9] enabling all-solid-state lithium ion batteries with very high cycling and rate performances.[5,10−13] However, a very thick solid electrolyte (∼ 0.5−1.0 mm) was usually used in these ASSLBs.[5,14−18] As a result, the cell-level energy densities of these ASSLBs are still limited to <200 Wh kg^{-1}, which is lower than that of the commercialized lithium ion batteries.

There are many reports about preparing thin electrolyte layers.[19−24] For example, Lee prepared a 64 μm thick electrolyte by creating a solid electrolyte-in-polymer matrix.[19] Jung reported the fabrication of a 70 μm thick sulfide electrolyte using a poly(*para*-phenylene terephthalamide) nonwoven scaffold as a mechanical support.[20] In addition, a submicrometer solid electrolyte membrane was also prepared using a self-assembly approach.[21] However, integrating these thin electrolytes into a high-energy cell (e.g., Li/S) has never been achieved because the thin electrolyte layer is easy to break during cell fabrication or operation, especially for the S cathode and Li anode with a large volume change. Therefore, the cathode materials used in these cells are $LiCoO_2$ and FeS_2, while the anode materials are graphite, $Li_4Ti_5O_{12}$, and Li−In alloy,[19,20] limiting the energy densities of ASSLBs.

In this present study, we report a method for fabricating cathode-supported ASSLBs with a thin electrolyte. Different from the conventional electrolyte-supported cell that starts from fabrication of the electrolyte layer and then the assembly of electrode layers on each side of the electrolyte, we start to build the cell from a stainless steel (SS)-supported Li_2S cathode. Using a Kevlar nonwoven scaffold as mechanical support, a ∼100 μm thick Li_3PS_4 (LPS) glass solid electrolyte was successfully integrated in the Li/S ASSLBs. The all-solid-state Li/S batteries with a Li_2S loading of 2.54 mg cm^{-2} provided a high initial capacity of 949.9 mAh g^{-1} at 0.05 C at room temperature. Moreover, the cell also exhibited great

Received: February 25, 2019
Accepted: April 12, 2019
Published: April 12, 2019

DOI: 10.1021/acsenergylett.9b00430
ACS Energy Lett. 2019, 4, 1073−1079

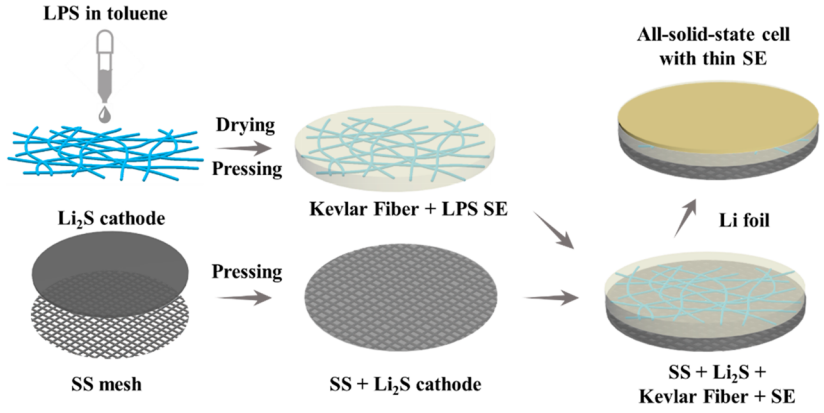

Figure 1. Schematic illustration of the fabrication of the cathode-supported all-solid-state cell with a thin sulfide electrolyte.

performance when increasing the loading of Li_2S to 7.64 mg cm^{-2}, and a high energy density of 370.6 Wh kg^{-1} at the cell level (excluding current collectors) was achieved. Our work provides a new approach for fabricating ASSLIBs with high energy densities.

Figure 1 shows a schematic illustration of the fabrication process of an all-solid-state cell with thin sulfide electrolytes. A Li_2S–LiI solid solution is used as the active material for the cathode because adding LiI into Li_2S can effectively improve the ionic conductivity of Li_2S,[25] which helps to improve the kinetics of the cathode. The ionic conductivity of the as-prepared Li_2S–LiI is measured to be 2.6×10^{-6} S cm^{-1} (Figure S1), which is about 2 orders of magnitude higher than that of Li_2S.[26] The active material is mixed with vapor-grown carbon fiber (VGCF) and a LPS glass electrolyte with a weight ratio of 75:10:15 to make the cathode. Detailed characterizations of the cathode composite can be found in the Supporting Information (Figures S2–S4). The main peaks in the XRD pattern (Figure S2) can be well indexed to Li_2S, implying the formation of Li_2S–LiI solid solution. The particle size of the composite is 0.5–5 μm from the SEM image (Figure S3). Elemental mappings of S, P, and I (Figure S4) indicate that the active material and solid electrolyte are uniformly distributed in the cathode composite. The content of Li_2S in the cathode composite is 43.4 wt %, which is the highest among all of the reported Li_2S-based cathodes in all-solid-state batteries.[27−32] The obtained cathode powders were mixed with polytetrafluoroethylene (PTFE) binder, ground in a mortar, and then rolled into thin sheets. The as-prepared cathode film was then cold-pressed onto a SS mesh current collector. The thin electrolyte layer was prepared by dropping LPS suspension in toluene into a Kevlar nonwoven scaffold, followed by drying overnight under vacuum. Toluene was used as the solvent to prepare the suspension because of its stability with the LPS electrolyte[20] as no other peaks can be detected in the XRD of the soaked LPS and all of the Raman peaks of the soaked LPS electrolyte are well matched with pristine LPS powders (Figure S5). Figure S6 shows SEM images of the LPS–Kevlar membrane after cold pressing, indicating that the membrane is very compact. The ionic conductivity of the LPS–Kevlar membrane is 0.30 mS cm^{-1} (Figure S7), which is slightly lower than that of the pristine LPS pellet (0.56 mS cm^{-1}) because the Kevlar nonwoven scaffold is an ionic insulator. The LPS–Kevlar electrolyte was cold pressed on the cathode film, and then, a thin Li metal was attached to the top side of the solid electrolyte to make an all-solid-state full cell. The stable voltage profiles of the Li/LPS–Kevlar/Li cell at 0.2 mA cm^{-2} (Figure S8) imply good interfacial stability between the LPS–Kevlar electrolyte and Li. It should be noted that LPS is not thermodynamically stable with Li,[33] and therefore, the interfacial stability should be achieved by the formation of a passivation interphase. A schematic of such an all-solid-state cell is shown in Figure 2.

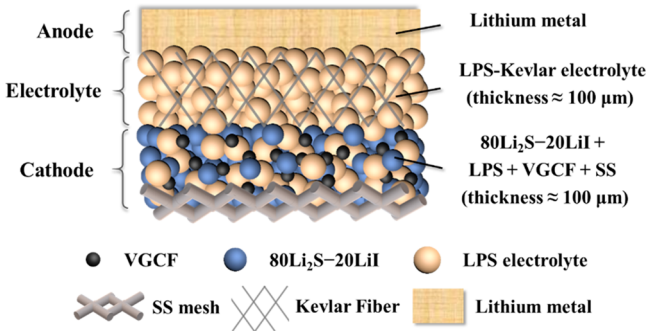

Figure 2. Schematic of the cathode-supported all-solid-state Li–Li_2S cell.

A photograph and SEM images of the key steps in the fabrication processes of all-solid-state cells are shown in Figure 3. A SS mesh with a pore size of around 200 μm (Figure 3a,b) was used as the current collector to enhance the mechanical strength and the integrity of the Li_2S cathode. The unique mesh structure of the current collector allows a high loading of active material (Li_2S: 2.54–7.64 mg cm^{-2}). The Li_2S–LiI active material is uniformly spread on the SS mesh (Figure 3c,d). The web structure of the Kevlar nonwoven scaffold is shown in Figure 3e,f. LPS suspension was prepared in an argon-filled glovebox (Figure 3g), and the dried LPS particles are homogeneous and regular, with sizes of approximately 2–5 μm (Figure 3h). The LPS suspension was dropped into a Kevlar nonwoven scaffold with a designed amount to control the thickness of solid electrolytes. Figure 3i,j shows a photograph and SEM image of the cold-pressed LPS–Kevlar membrane, which clearly shows the reinforced structure.

The thicknesses of the electrolyte membrane and the cathode layer were demonstrated from cross-sectional SEM images (Figures 3k,l and 4a,b). The distribution of the elements from the EDS mappings in Figure 4d–i shows that the thicknesses of the cathode layer and the electrolyte layer are both about 100 μm as Fe, F, and I are present only in the

DOI: 10.1021/acsenergylett.9b00430
ACS Energy Lett. 2019, 4, 1073−1079

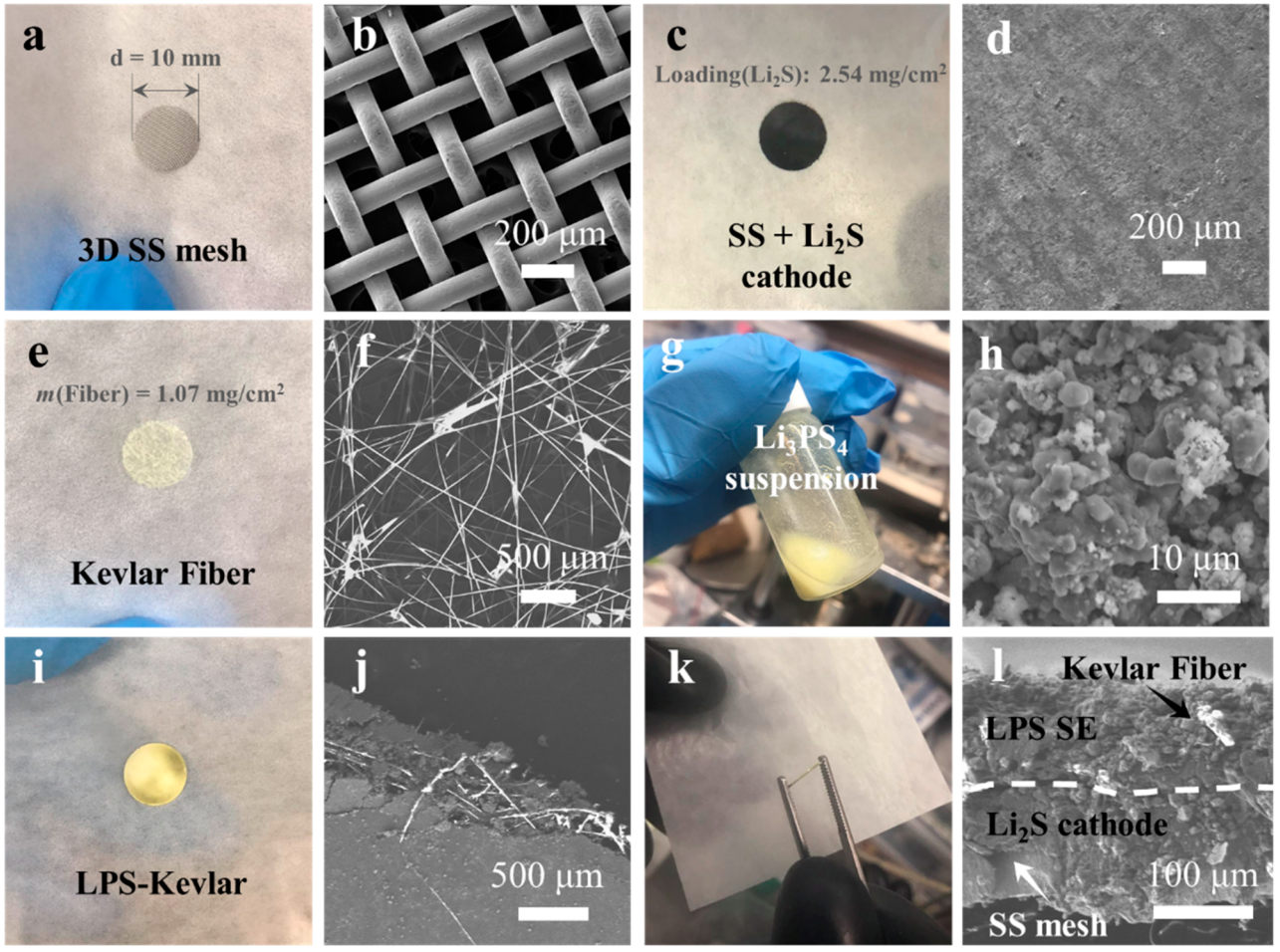

Figure 3. Photos and SEM images of (a,b) SS mesh, (c,d) a SS−Li_2S composite cathode, (e,f) a Kevlar nonwoven scaffold, (g) a Li_3PS_4 electrolyte suspension, (h) Li_3PS_4 dried from the suspension, (i,j) a Li_3PS_4−Kevlar electrolyte, and (k,l) a SS mesh-supported cathode and Li_3PS_4−Kevlar electrolyte.

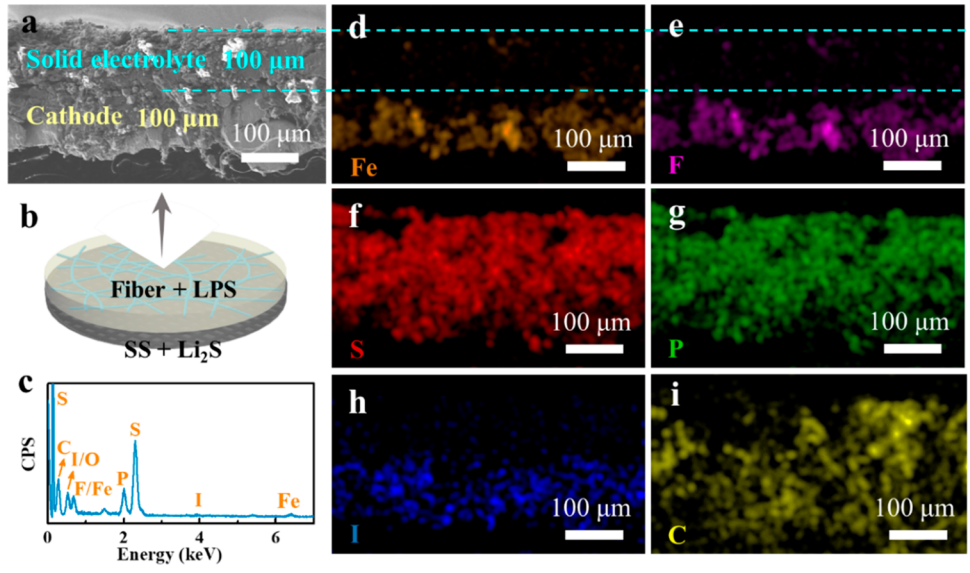

Figure 4. (a) Cross-sectional SEM image, (b) schematic illustration, and (c) EDS of the cathode composite. (d−i) Element mappings of Fe, F, S, P, I, and C.

cathode and P and S are present in both the cathode and the electrolyte. Furthermore, the energy dispersive spectroscopy (EDS) results in Figure 4c confirm the high purity of the sample.

DOI: 10.1021/acsenergylett.9b00430
ACS Energy Lett. 2019, 4, 1073−1079

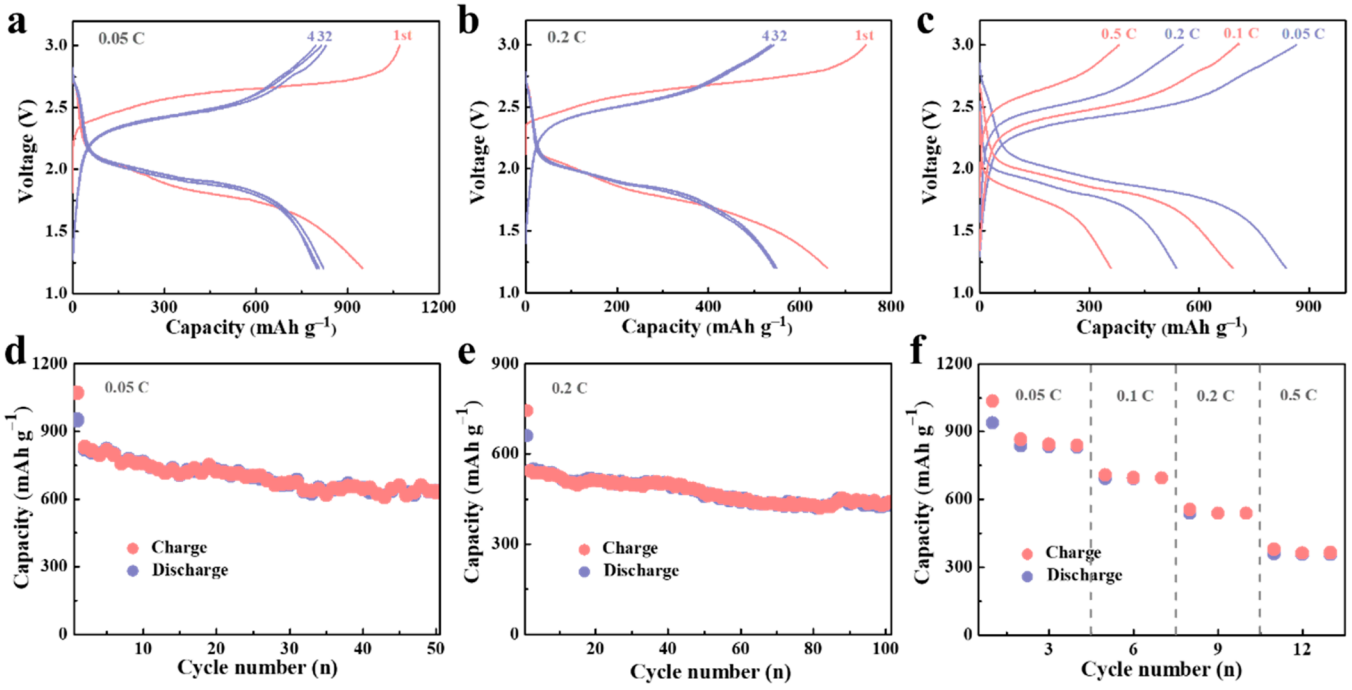

Figure 5. Charge−discharge profiles of the cathode-supported all-solid-state Li−Li_2S cells at (a) 0.05 C, (b) 0.2 C, and (c) different rates from 0.05 to 0.5 C at 25 °C. Cycle performance of the cathode-supported all-solid-state Li−Li_2S cells at (d) 0.05 and (e) 0.2 C at 25 °C. (f) Rate performance of the cathode-supported all-solid-state Li−Li_2S cell at 25 °C. The specific capacities are calculated based on the mass of Li_2S in the cathode composite. The Li_2S loading is 2.54 mg cm^{-2}.

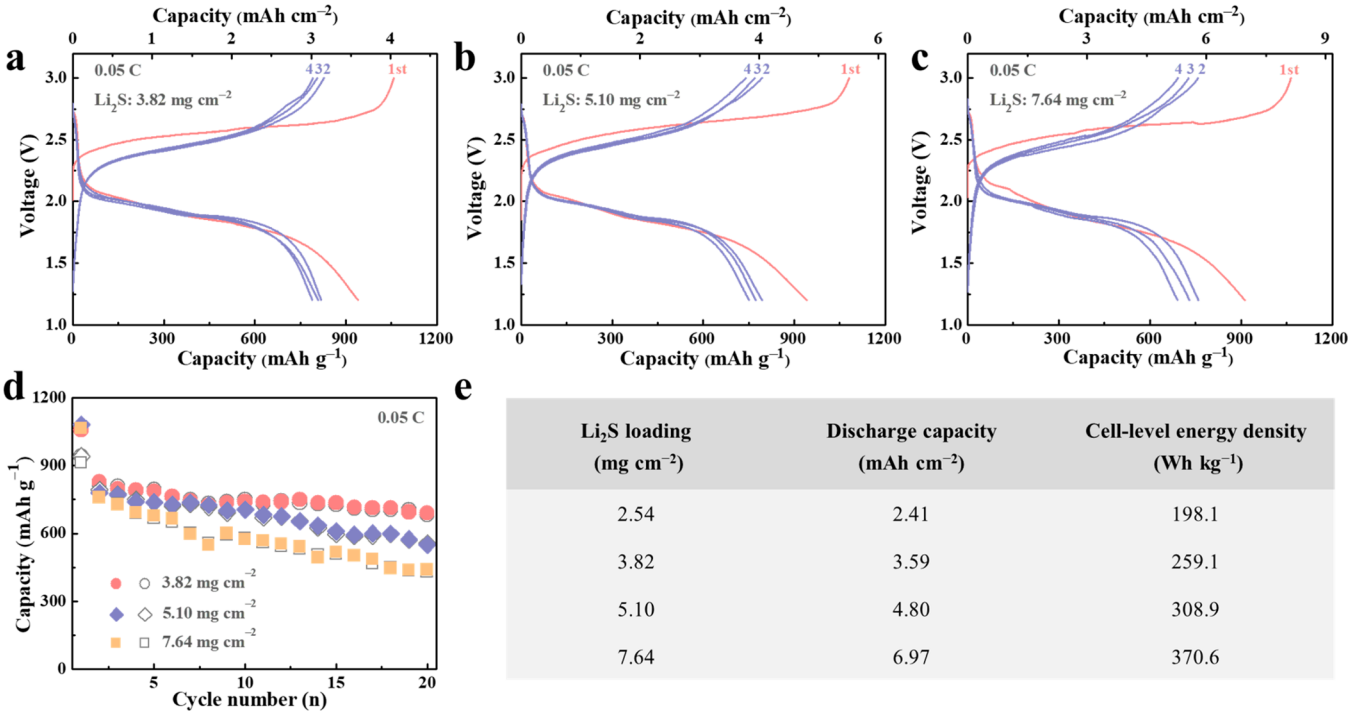

e

Li_2S loading (mg cm^{-2})	Discharge capacity (mAh cm^{-2})	Cell-level energy density (Wh kg^{-1})
2.54	2.41	198.1
3.82	3.59	259.1
5.10	4.80	308.9
7.64	6.97	370.6

Figure 6. Charge−discharge profiles of the cathode-supported all-solid-state Li−Li_2S cells with Li_2S loadings of (a) 3.82, (b) 5.10, and (c) 7.64 mg cm^{-2} at 0.05 C at 25 °C. (d) Cycle performance of the cathode-supported all-solid-state Li−Li_2S cells with different Li_2S loadings. (e) Cell-level energy densities of the cathode-supported all-solid-state Li−Li_2S cells with different loadings.

The electrochemical performances of all-solid-state full cells were evaluated at room temperature. Figure 5a shows the galvanostatic charge−discharge profiles of the Li−Li_2S solid cell with a Li_2S loading of 2.54 mg cm^{-2} in the potential range of 1.2−3.0 V at 0.05 C at room temperature. Different from the traditional liquid Li−Li_2S cell, only one plateau is observed during charge and discharge processes. No polysulfide intermediates are formed during the conversion reaction that completely solves the issue of shuttle reaction in a liquid Li−Li_2S cell.[25,30,34] The cell in the first charge−discharge process

DOI: 10.1021/acsenergylett.9b00430
ACS Energy Lett. 2019, 4, 1073−1079

displays a charge capacity of 1070.1 mAh g^{-1} and a high discharge capacity of 949.9 mAh g^{-1} with a Coulombic efficiency of 88.8%. The relatively large overpotential in the first cycle is attributed to the activation process.[25] During the following cycles, the overpotential decreases, although it is still relatively large when compared with the cells using $LiCoO_2$ as the cathode.[5] Possible reasons for the large overpotential include the addition of PTFE binder in the cathode composite and the low ionic conductivity of the electrolyte. The cell capacity is slightly reduced with charge−discharge cycles (Figure 5d). At 50 cycles, the all-solid-state cell with thin electrolyte still shows a high discharge capacity of 636.4 mAh g^{-1}. The excellent capacity retention of the solid cell benefits from the SS mesh current collector. The galvanostatic charge−discharge performance of the cell without the SS mesh current collector was also tested (Figure S9a). The cell showed a low initial discharge capacity of 840.5 mAh g^{-1} with a poor cycle performance and large cell resistance (Figure S9b and S10) at 50 cycles. The results show that using a SS mesh current collector effectively improves the mechanical integrity of the Li_2S cathode that experiences a huge volume change during the charge−discharge process. The cycle performance of the cell at a high rate of 0.2 C is shown in Figure 5b,e. Although the increase of the current rate from 0.05 to 0.2 C reduces the discharge capacity and enhances the overpotential, the cell still shows high cycling stability at a capacity decay rate of only 1.16 mAh g^{-1} per cycle from cycle 2 to cycle 100. In addition, the active cell exhibits a high rate capability at 25 °C (Figure 5c,f). Discharge capacities of 836.9, 692.2, 537.8, and 358.5 mAh g^{-1} are achieved at 0.05, 0.1, 0.2, and 0.5 C, respectively. As one important advantage of all-solid-state batteries is the ability to operate at higher temperatures, we also tested the electrochemical performance of the cell at 60 °C (Figure S11). The cell was able to cycle stably at 0.1 and 0.2 C at 60 °C with enhanced kinetics.

We further tested the electrochemical performance of the cells with increased Li_2S loadings. The galvanostatic charge−discharge profiles with Li_2S loadings of 3.82, 5.10, and 7.64 mg cm^{-2} are shown in Figure 6a−c. The initial discharge capacities of the three cells with different Li_2S loading are similar; however, the cell with a higher Li_2S loading shows a faster capacity decay (Figure 6d). The cell energy densities with different Li_2S loadings are summarized in Figure 6e.

Figure 7 compares the cell energy densities of all of the reported sulfide-based all-solid-state cells, with the detailed weights of the cell components shown in Table S1. The cell energy density is calculated from the average discharge voltage, cell capacity, and total weights of the cathode, solid electrolyte, and anode, but the weights of the current collectors and exterior package are excluded for calculation due to lack of information from the literature. One reason is that most of the previous reports used a lab-scale Swagelok cell to test the performance of the solid-state battery, wherein two SS (or Ti) rods were used as the current collectors.[32,35] As shown in the figure, the cell energy densities of most reported all-solid-state cells with sulfide electrolytes are <100 Wh kg^{-1}, which is much lower than that of commercialized liquid cells of ∼ 200 Wh kg^{-1} due to utilization of thick solid electrolytes. Our Li−Li_2S solid cell with a high Li_2S loading of 7.64 mg cm^{-2} exceeds an energy density of 370 Wh kg^{-1} at the cell level for the first cycle, which is the highest energy density reported to date. It should be noted that the cell-level energy density of the cell is not high if the weight of the SS mesh current collector is included in the calculation. Because the main purpose of using SS mesh as the current collector is to provide a matrix for the cathode composite, other electronically conducting materials with a 2D or 3D structure but with a lower density can also be used as current collectors. For example, the cell-level energy density (including current collectors) of the cell was largely increased (from 59 to 159 Wh kg^{-1}) by replacing the SS mesh (53.3 mg cm^{-2}) with Ni-coated Kevlar fiber (1.22 mg cm^{-2}) as the current collector (Figure S12).

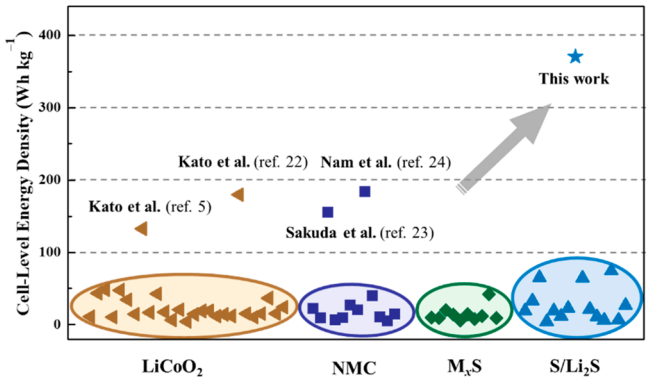

Figure 7. Cell-level energy density of all-solid-state cells using sulfides as the electrolyte. The cells with different cathodes are represented with different colors. More detailed information about the cells can be found in Table S1. Note that the weight of the current collectors was not included in the calculation, and the cell-level energy density of this work is calculated based on the reversible capacity of the first cycle.

In summary, we demonstrate thick cathode-supported ASSLBs with a thin electrolyte (∼100 μm). LPS−Kevlar solid electrolyte membranes are formed by dropping the LPS suspension into the Kevlar nonwoven scaffold followed by drying/cold pressing onto a thick SS mesh-supported Li_2S−LiI cathode. Using a Li metal anode, the Li−Li_2S cell with 2.54 mg cm^{-2} Li_2S loading achieves a high reversible discharge capacity of 949.9 mAh g^{-1} at 0.05 C and stable cycling for 100 cycles at 0.2 C. The all-solid-state Li−Li_2S cell with a high Li_2S loading of 7.64 mg cm^{-2} exhibits an extremely high cell-level energy density of 370.6 Wh kg^{-1}.

■ ASSOCIATED CONTENT

Supporting Information

The Supporting Information is available free of charge on the ACS Publications website at DOI: 10.1021/acsenergylett.9b00430.

Impedance plot of the SS/80Li_2S-20LiI/SS cell, XRD pattern and SEM images of the cathode composite, XRD patterns and Raman spectra of the as-prepared LPS and LPS dried from the LPS suspension in toluene, SEM images of the surface of the LPS−Kevlar electrolyte, Nyquist plots of blocking cells, galvanostatic cycling of the Li/LPS−Kevlar/Li cell, charge−discharge profiles and cycle performance of Li−Li_2S solid cells without a SS mesh current collector, Nyquist plots of the Li−Li_2S cells, charge−discharge profiles of the cathode-supported all-solid-state Li−Li_2S cells at 60 °C, charge−discharge of the all-solid-state Li−Li_2S cell with Ni-coated Kevlar nonwoven as the current collector for the cathode, and summary of the cell-level energy densities of all-solid-state cells using sulfides as the electrolyte (PDF)

DOI: 10.1021/acsenergylett.9b00430
ACS Energy Lett. 2019, 4, 1073−1079

AUTHOR INFORMATION

Corresponding Authors

*E-mail: fdhan@umd.edu.
*E-mail: piliu@eng.ucsd.edu.
*E-mail: cswang@umd.edu.

ORCID

Jiangping Tu: 0000-0002-7928-1583
Ping Liu: 0000-0002-1488-1668
Chunsheng Wang: 0000-0002-8626-6381

Notes

The authors declare no competing financial interest.

ACKNOWLEDGMENTS

This work is supported by the U.S. Department of Energy ARPA-E (Award No. DE-AR0000781).

REFERENCES

(1) Hu, Y.-S. Batteries: Getting Solid. *Nature Energy* **2016**, *1* (4), 16042.
(2) Janek, J.; Zeier, W. G. A Solid Future for Battery Development. *Nature Energy* **2016**, *1* (9), 16141.
(3) Li, J. C.; Ma, C.; Chi, M. F.; Liang, C. D.; Dudney, N. J. Solid Electrolyte: the Key for High-Voltage Lithium Batteries. *Adv. Energy Mater.* **2015**, *5* (4), 1401408.
(4) Kamaya, N.; Homma, K.; Yamakawa, Y.; Hirayama, M.; Kanno, R.; Yonemura, M.; Kamiyama, T.; Kato, Y.; Hama, S.; Kawamoto, K.; et al. Lithium Superionic Conductor. *Nat. Mater.* **2011**, *10* (9), 682−686.
(5) Kato, Y.; Hori, S.; Saito, T.; Suzuki, K.; Hirayama, M.; Mitsui, A.; Yonemura, M.; Iba, H.; Kanno, R. High-Power All-Solid-State Batteries Using Sulfide Superionic Conductors. *Nat. Energy* **2016**, *1* (4), 16030.
(6) Seino, Y.; Ota, T.; Takada, K.; Hayashi, A.; Tatsumisago, M. A Sulphide Lithium Super Ion Conductor is Superior to Liquid Ion Conductors for Use in Rechargeable Batteries. *Energy Environ. Sci.* **2014**, *7* (2), 627−631.
(7) Mizuno, F.; Hayashi, A.; Tadanaga, K.; Tatsumisago, M. New, Highly Ion-Conductive Crystals Precipitated from Li_2S−P_2S_5 Glasses. *Adv. Mater.* **2005**, *17* (7), 918−921.
(8) Kanno, R.; Murayama, M. Lithium Ionic Conductor Thio-LISICON: The Li_2S-GeS_2-P_2S_5 System. *J. Electrochem. Soc.* **2001**, *148* (7), A742−A746.
(9) Zhou, L.; Park, K.-H.; Sun, X.; Lalère, F.; Adermann, T.; Hartmann, P.; Nazar, L. F. Solvent-Engineered Design of Argyrodite Li_6PS_5X (X = Cl, Br, I) Solid Electrolytes with High Ionic Conductivity. *ACS Energy Letters* **2019**, *4* (1), 265−270.
(10) Yao, X. Y.; Huang, N.; Han, F. D.; Zhang, Q.; Wan, H. L.; Mwizerwa, J. P.; Wang, C. S.; Xu, X. X. High-Performance All-Solid-State Lithium-Sulfur Batteries Enabled by Amorphous Sulfur-Coated Reduced Graphene Oxide Cathodes. *Adv. Energy Mater.* **2017**, *7* (17), 1602923.
(11) Han, F.; Yue, J.; Fan, X.; Gao, T.; Luo, C.; Ma, Z.; Suo, L.; Wang, C. High-Performance All-Solid-State Lithium-Sulfur Battery Enabled by a Mixed-Conductive Li_2S Nanocomposite. *Nano Lett.* **2016**, *16* (7), 4521−4527.
(12) Nagata, H.; Chikusa, Y. A Lithium Sulfur Battery with High Power Density. *J. Power Sources* **2014**, *264*, 206−210.
(13) Moon, C. K.; Lee, H.-J.; Park, K. H.; Kwak, H.; Heo, J. W.; Choi, K.; Yang, H.; Kim, M.-S.; Hong, S.-T.; Lee, J. H.; et al. Vacancy-Driven Na^+ Superionic Conduction in New Ca-Doped Na_3PS_4 for All-Solid-State Na-Ion Batteries. *ACS Energy Letters* **2018**, *3* (10), 2504−2512.
(14) Suzuki, K.; Kato, D.; Hara, K.; Yano, T.-A.; Hirayama, M.; Hara, M.; Kanno, R. Composite Sulfur Electrode Prepared by High-Temperature Mechanical Milling for use in an All-Solid-State Lithium-Sulfur Battery with a $Li_{3.25}Ge_{0.25}P_{0.75}S_4$ Electrolyte. *Electrochim. Acta* **2017**, *258*, 110−115.
(15) Busche, M. R.; Weber, D. A.; Schneider, Y.; Dietrich, C.; Wenzel, S.; Leichtweiss, T.; Schröder, D.; Zhang, W.; Weigand, H.; Walter, D.; et al. In Situ Monitoring of Fast Li-Ion Conductor $Li_7P_3S_{11}$ Crystallization Inside a Hot-Press Setup. *Chem. Mater.* **2016**, *28* (17), 6152−6165.
(16) Lin, Z.; Liu, Z.; Fu, W.; Dudney, N. J.; Liang, C. Lithium Polysulfidophosphates: A Family of Lithium-Conducting Sulfur-Rich Compounds for Lithium-Sulfur batteries. *Angew. Chem., Int. Ed.* **2013**, *52* (29), 7460−7463.
(17) Nagata, H.; Chikusa, Y. All-Solid-State Lithium-Sulfur Battery with High Energy and Power Densities at the Cell Level. *Energy Technol.* **2016**, *4* (4), 484−489.
(18) Lin, Z.; Liu, Z.; Dudney, N. J.; Liang, C. Lithium Superionic Sulfide Cathode for All-Solid Lithium−Sulfur Batteries. *ACS Nano* **2013**, *7* (3), 2829−2833.
(19) Whiteley, J. M.; Taynton, P.; Zhang, W.; Lee, S. H. Ultra-thin Solid-State Li-Ion Electrolyte Membrane Facilitated by a Self-Healing Polymer Matrix. *Adv. Mater.* **2015**, *27* (43), 6922−6927.
(20) Nam, Y. J.; Cho, S. J.; Oh, D. Y.; Lim, J. M.; Kim, S. Y.; Song, J. H.; Lee, Y. G.; Lee, S. Y.; Jung, Y. S. Bendable and Thin Sulfide Solid Electrolyte Film: A New Electrolyte Opportunity for Free-Standing and Stackable High-Energy All-Solid-State Lithium-Ion Batteries. *Nano Lett.* **2015**, *15* (5), 3317−3323.
(21) Hood, Z. D.; Wang, H.; Pandian, A. S.; Peng, R.; Gilroy, K. D.; Chi, M.; Liang, C.; Xia, Y. Fabrication of Sub-Micrometer-Thick Solid Electrolyte Membranes of β-Li_3PS_4 via Tiled Assembly of Nanoscale, Plate-Like Building Blocks. *Adv. Energy Mater.* **2018**, *8* (21), 1800014.
(22) Kato, Y.; Shiotani, S.; Morita, K.; Suzuki, K.; Hirayama, M.; Kanno, R. All-Solid-State Batteries with Thick Electrode Configurations. *J. Phys. Chem. Lett.* **2018**, *9* (3), 607−613.
(23) Sakuda, A.; Kuratani, K.; Yamamoto, M.; Takahashi, M.; Takeuchi, T.; Kobayashi, H. All-Solid-State Battery Electrode Sheets Prepared by a Slurry Coating Process. *J. Electrochem. Soc.* **2017**, *164* (12), A2474−A2478.
(24) Nam, Y. J.; Oh, D. Y.; Jung, S. H.; Jung, Y. S. Toward Practical All-Solid-State Lithium-Ion Batteries with High Energy Density and Safety: Comparative Study for Electrodes Fabricated by Dry- and Slurry-Mixing Processes. *J. Power Sources* **2018**, *375*, 93−101.
(25) Hakari, T.; Hayashi, A.; Tatsumisago, M. Li_2S-Based Solid Solutions as Positive Electrodes with Full Utilization and Superlong Cycle Life in All-Solid-State Li/S Batteries. *Adv. Sustainable Syst.* **2017**, *1* (6), 1700017.
(26) Hakari, T.; Hayashi, A.; Tatsumisago, M. Highly Utilized Lithium Sulfide Active Material By Enhancing Conductivity In All-Solid-State Batteries. *Chem. Lett.* **2015**, *44* (12), 1664−1666.
(27) Takeuchi, T.; Kageyama, H.; Nakanishi, K.; Ohta, T.; Sakuda, A.; Sakaebe, H.; Kobayashi, H.; Tatsumi, K.; Ogumi, Z. Rapid Preparation of Li_2S-P_2S_5 Solid Electrolyte and Its Application for Graphite/Li_2S All-Solid-State Lithium Secondary Battery. *ECS Electrochem. Lett.* **2014**, *3* (5), A31−A35.
(28) Nagao, M.; Hayashi, A.; Tatsumisago, M. Sulfur−Carbon Composite Electrode for All-Solid-State Li/S Battery with Li_2S−P_2S_5 Solid Electrolyte. *Electrochim. Acta* **2011**, *56* (17), 6055−6059.
(29) Yang, Y.; Zheng, G.; Misra, S.; Nelson, J.; Toney, M. F.; Cui, Y. High-Capacity Micrometer-Sized Li_2S Particles as Cathode Materials for Advanced Rechargeable Lithium-Ion Batteries. *J. Am. Chem. Soc.* **2012**, *134* (37), 15387−15394.
(30) Nagao, M.; Hayashi, A.; Tatsumisago, M. High-Capacity Li_2S−Nanocarbon Composite Electrode for All-Solid-State Rechargeable Lithium Batteries. *J. Mater. Chem.* **2012**, *22* (19), 10015−10020.
(31) Hayashi, A.; Ohtsubo, R.; Ohtomo, T.; Mizuno, F.; Tatsumisago, M. All-Solid-State Rechargeable Lithium Batteries with Li_2S as a Positive Electrode Material. *J. Power Sources* **2008**, *183* (1), 422−426.
(32) Nagao, M.; Hayashi, A.; Tatsumisago, M.; Ichinose, T.; Ozaki, T.; Togawa, Y.; Mori, S. Li_2S Nanocomposites Underlying High-

DOI: 10.1021/acsenergylett.9b00430
ACS Energy Lett. 2019, 4, 1073−1079

Capacity and Cycling Stability in All-Solid-State Lithium−Sulfur Batteries. *J. Power Sources* **2015**, *274*, 471−476.
(33) Han, F. D.; Zhu, Y. Z.; He, X. F.; Mo, Y. F.; Wang, C. S. Electrochemical Stability of $Li_{10}GeP_2S_{12}$ and $Li_7La_3Zr_2O_{12}$ Solid Electrolytes. *Adv. Energy Mater.* **2016**, *6* (8), 1501590.
(34) Mikhaylik, Y. V.; Akridge, J. R. Polysulfide Shuttle Study in the Li/S Battery System. *J. Electrochem. Soc.* **2004**, *151* (11), A1969−A1976.
(35) Aso, K.; Sakuda, A.; Hayashi, A.; Tatsumisago, M. All-Solid-State Lithium Secondary Batteries Using NiS-Carbon Fiber Composite Electrodes Coated With Li_2S-P_2S_5 Solid Electrolytes By Pulsed Laser Deposition. *ACS Appl. Mater. Interfaces* **2013**, *5* (3), 686−690.

DOI: 10.1021/acsenergylett.9b00430
ACS Energy Lett. 2019, 4, 1073−1079